Title

Multi-Ratio Operation of Flying Capacitor Multilevel Converters At and Above Resonance

ISBN

9798350399882

Authors

Abramson, Rose A
Coday, Samantha
Brooks, Nathan C
et al.

Publication Date

2022-12-08

DOI

10.1109/spec55080.2022.10058297

2022 IEEE 7th Southern Power Electronics Conference (SPEC), Nadi, Fiji, December 2022

Multi-Ratio Operation of Flying Capacitor Multilevel Converters At and Above Resonance

R. A. Abramson
S. Coday
N. C. Brooks
M. E. Blackwell
N. M. Ellis
R. C. N. Pilawa-Podgurski

Multi-Ratio Operation of Flying Capacitor Multilevel Converters At and Above Resonance

Rose A. Abramson
Dept. of Elec. Eng. and Comp. Sci.
University of California, Berkeley
Berkeley, USA
rose_abramson@berkeley.edu

Samantha Coday
Dept. of Elec. Eng. and Comp. Sci.
University of California, Berkeley
Berkeley, USA
scoday@berkeley.edu

Nathan C. Brooks
Dept. of Elec. Eng. and Comp. Sci.
University of California, Berkeley
Berkeley, USA
nathanbrooks@berkeley.edu

Margaret E. Blackwell
Dept. of Elec. Eng. and Comp. Sci.
University of California, Berkeley
Berkeley, USA
blackwell@berkeley.edu

Nathan M. Ellis
Dept. of Elec. Eng. and Comp. Sci.
University of California, Berkeley
Berkeley, USA
nathanmilesellis@berkeley.edu

Robert C. N. Pilawa-Podgurski
Dept. of Elec. Eng. and Comp. Sci.
University of California, Berkeley
Berkeley, USA
pilawa@berkeley.edu

***Abstract*—The flying capacitor multilevel (FCML) converter is an attractive candidate for dc/dc step-up and step-down applications due to its relatively low switch stress and greatly reduced inductor volume. It can be operated in either a regulating pulse width modulated (PWM) or fixed-ratio resonant mode. For fixed-ratio operation, the FCML converter is capable of achieving multiple rational conversion ratios (up to a maximum of N:1) with the same switch-capacitor network simply by changing the gating signals of its switches. In addition, the inductance requirement can be further reduced compared to regulated operation, while switching losses at resonance can be mitigated due to the presence of soft-switching. However, there is limited prior analysis of higher level-count ($N \geq 3$) fixed-ratio FCML converters operating at resonance or above resonance, where the derivation of appropriate phase durations becomes significantly more involved. This work presents a full analytical method to calculate optimal phase durations for the fixed-ratio FCML converter across all rational conversion ratios while operating at or above resonance. Hardware results for an $N = 5$ FCML converter are presented for conversion ratios 5:1, 5:2, 5:3 and 5:4, illustrating the ability to use above-resonance operation to optimize the distribution of switching losses and conduction losses in the converter.**

I. Introduction

THE flying capacitor multilevel (FCML) converter, shown in Fig. 1, has become a popular candidate for both step-up and step-down conversion due to its high power density, high efficiency and wide output range [1]–[3]. The FCML topology is often presented as an attractive alternative to conventional buck- or boost-type topologies because of its greatly reduced inductance requirements and decreased voltage rating of the switching devices. The lower switch-voltage ratings allow for the use of devices with lower on-resistance or gate/output capacitance [4]. This reduction in parasitic losses can often outweigh any increased losses due to a higher number of switches, allowing for high efficiency operation.

979-8-3503-9988-2/22/$31.00 2022 IEEE

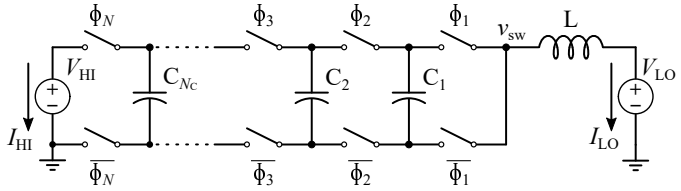

Fig. 1: Schematic for a generic $N{:}M$ FCML converter

While the FCML converter can be operated in a pulse-width-modulated (PWM) mode, similar to a buck or boost converter, it can also be operated resonantly as a fixed-ratio converter [5], [6]. In its resonant mode, the FCML converter operates similarly to other hybrid resonant switched-capacitor (SC) converters, specifically those of the "inductor-at-output" form, as defined in [7][1]. In addition, the FCML converter can be operated with multiple rational $N{:}M$ conversion ratios, as described in [8].

One of the main benefits of hybrid SC converters is the elimination of the capacitor charge sharing loss present in conventional SC converters, through the use of an assistive inductor that resonates with the flying capacitors, as discussed in [9], [10]. Compared to a conventional switched-inductor converter, the inductor in a resonant hybrid SC converter is subjected to significantly reduced volt-seconds and can subsequently be made much smaller [11]. Reference [11] further explores how the total passive volume (including both capacitors and inductors) of these hybrid SC converters can be optimized, resulting in much higher power densities than seen with a traditional buck converter. Furthermore, resonant operation allows for zero current or zero voltage switching (ZCS/ZVS), thereby reducing switching losses [12], [13].

Prior literature has explored operating "inductor-at-output"

[1]The referenced work only considered step-down converters. A more general terminology would be "inductor-at-low-side-port," which would be the input port for a step-up converter. This construction is also referred to as a "direct" structure in [5], [6].

hybrid SC converters at switching frequencies higher than the natural resonant frequency of the circuit, while maintaining segmented sinusoidal currents and voltages as the inductor is pushed into a continuous forward conduction mode. When operating above resonance—i.e., as the converter approaches the fast-switching-limit (FSL) [14]—the output impedance of the converter reduces from the at- or below-resonant cases, corresponding to a reduction in conduction losses [6], [15]. This operating mode is not achievable with tank-based or "indirect" converters [5], [6], whose output impedance is a minimum only at resonance. Subsequently, "inductor-at-output" converters are less sensitive to component or frequency variation, often omitting the need for complex control or dynamic calibration [12], [13].

When operating above resonance, conduction and ac losses in the switches and inductors are considerably reduced due to decreased rms currents. For high-current applications, the reduction in these losses significantly outweigh any increased switching losses due to the loss of ZCS—i.e., overlap losses due to non-zero current at the switching transitions.

Unlike many other hybrid SC converters, the resonant FCML requires multi-resonant operation in which the phase time durations not only depend on flying capacitance, inductance, and conversion ratio, but also on the ratio of switching frequency to the natural resonant frequency. In [5], [15], phase time durations were given for a general $2:1$ resonant converter (the ratio at which all hybrid SC converters collapse to the same topology). This work was not extended to higher order converters, where the phase duration relationships become significantly more complex. Prior work in [6] *did* explore higher order operation at and above resonance, for $N = 3$ and $N = 6$ FCML converters. However, no analytical closed-form solution was given for phase timings; instead, the authors developed a valley current control scheme to converge on optimal phase durations through active feedback.

Recent work in [16] presented an analytical method to calculate these time durations for resonant FCML converters, though it limited the scope to a conversion ratio of $N{:}\,1$. However, the FCML is capable of modulating the conversion ratio for a given switch-capacitor network of level N, such that it achieves a conversion of $N{:}\,1$ up to $N{:}\,(N-1)$. While the highest conversion ratio of $N{:}\,1$ may be the most suitable for large step-up or step-down applications, the FCML converter's multi-ratio capability extends the applicability to scenarios with very wide input/output voltage range.

This work proposes an analytical method to calculate appropriate phase timing durations for higher-level count FCML converters when operating with $N{:}\,M$ conversion ratios both at resonance and above resonance. These proposed timings are experimentally validated for an $N = 5$ FCML converter, showcasing operation both at the highest conversion ratio of 5:1, as well as at 5:2, 5:3, and 5:4.

II. Theory of Operation

Fig. 1 shows a generic step-down $N{:}\,M$ FCML converter, where the high-side and low-side voltage ports are denoted as V_{HI} and V_{LO}, respectively. Here, N refers to both the maximum integer conversion ratio of the FCML converter, as well as the number of complementary switch-pairs, $S_{N\mathrm{A/B}}$. In this work, multi-ratio operation is presented for $M \in \{1, 2, 3, \ldots, N-1\}$. The gate timings of each switch pair and the inductor current waveform for a general N-level, $M = 2$ FCML are shown in Fig. 2, where the rising edge of switch $S_{M\mathrm{A}}$ occurs at time $t = 0$ seconds and the presented phase ordering minimizes switching activity.

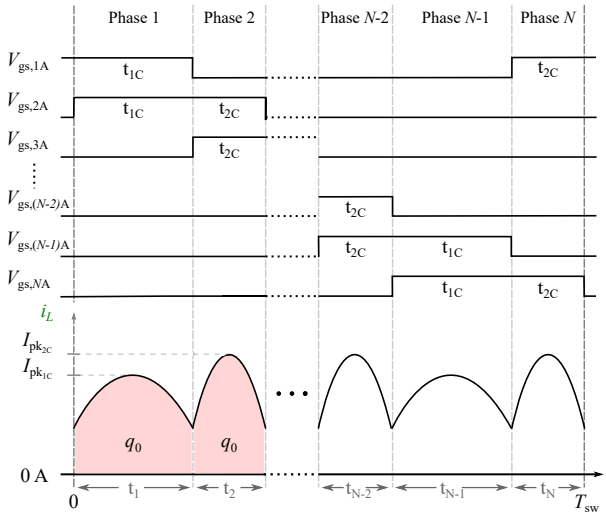

Fig. 2: Minimum switch activity modulation scheme at- and above-resonance for $N{:}\,M$ FCML where $M = 2$. The rising edge of switch $S_{M\mathrm{A}}$ occurs at time $t = 0$. The current i_{L} is shown for above-resonance.

For multi-ratio operation, each high-side 'A' switch conducts for M phases, and during any given phase M high-side switches are conducting. The on-times of each switch are adjusted to ensure a half-sine-wave resonant inductor current waveform for each switching phase when operating at resonance. When operating above resonance, the inductor current still has a half-sine-wave shape, though it will only follow the top arc of a sinusoid since the current no longer resonates fully down to zero. As the converter operates farther above resonance, the ratio of the peak current to output current, $\frac{I_{\mathrm{pk}}}{I_{\mathrm{out}}}$, decreases [16]. The current therefore follows a shorter (and flatter) segment of a rectified sine waveform, resulting in lower peak-to-peak current ripple. Current waveforms for a) at resonance, b) slightly above resonance, and c) far above resonance are shown in Fig. 3, illustrating this general trend.

The phase time durations can be calculated using the following analysis, which applies to any rational number $N{:}\,M$ conversion ratio. An example calculation is performed using the 5:2 step-down FCML converter depicted in Fig. 4. Here, the charge q_0 is a normalizing charge quantity used to relate the quantities of charge conducted through all elements using the charge flow analysis described in [14]. In this work, q_0 is chosen to be defined in terms of the converter operating parameters as $q_0 = I_{\mathrm{LO}}/(N \cdot f_{\mathrm{sw},0})$, where I_{LO} is the average low-side current, N is the number of levels, and $f_{\mathrm{sw},0}$ is the switching frequency of the converter at resonance.

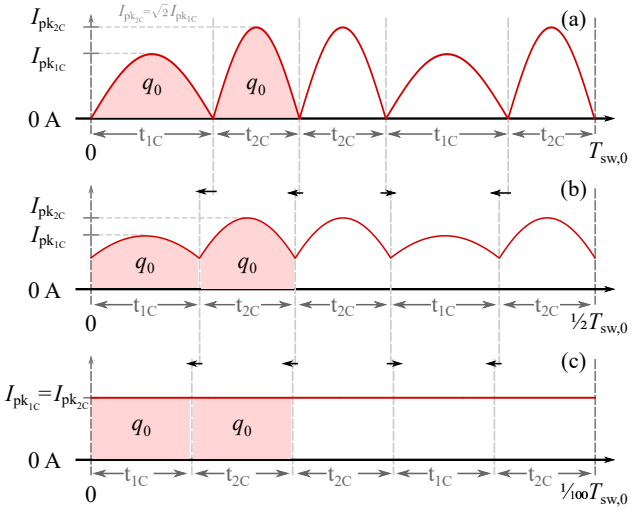

Fig. 3: Example 5:2 FCML inductor current waveforms at a) at resonance ($\Gamma = 1$), b) slightly above resonance ($\Gamma = 2$), and c) far above resonance ($\Gamma = 100$). Note that the peak current and time durations are different for each case. As the converter operates far above the natural resonance, all phase durations approach equal values ($t_{1C} = t_{2C}$).

Following the charge flow across phases, we see that each flying capacitor is charged by q_0 in one phase and discharged by q_0 in one other phase, thereby maintaining charge balance across the capacitors in periodic steady-state. Because each flying capacitor is charged/discharged by the same charge quantity, equating all capacitors C_1 through C_{N-1} to a singular value, C_0, enforces equal voltage ripple magnitude on each of the flying capacitors. The FCML converter does not require specific capacitor sizing to achieve soft charging, but setting all capacitance values to be equal can simplify the converter design. This assumption is also made in the analysis presented in [10]. Looking at Fig. 4, it can be seen that one q_0 quantity is delivered to the low-side voltage, V_{LO}, through inductor L during *each* of the five (i.e., N) phases, while one q_0 worth of charge is supplied by V_{HI} during *each* of Phase 4 and Phase 5. More generally, the net charge delivered to V_{LO} over N phases is $q_{LO} = Nq_0$ while the charge supplied by the source is $q_{HI} = Mq_0$, resulting in a voltage conversion ratio of $N{:}\,M$.

III. Calculating Phase Durations

To calculate appropriate timing durations for each phase in periodic steady-state, the inductor current is assumed to have the same value at each phase transition. This implies zero net volt-seconds across the inductor within *each* phase, as opposed to only over the total switching period. This constraint results in minimized rms current ripple over the whole period, and therefore minimized conduction and ac losses. Additionally, the converter is assumed to have a high Q-factor, such that the inductor and current waveforms are purely sinusoidal, with negligible damping.

The following analysis, performed for arbitrary M values, yields phase time durations that are independent of M and are the same as those presented for the $M = 1$ case in [16].

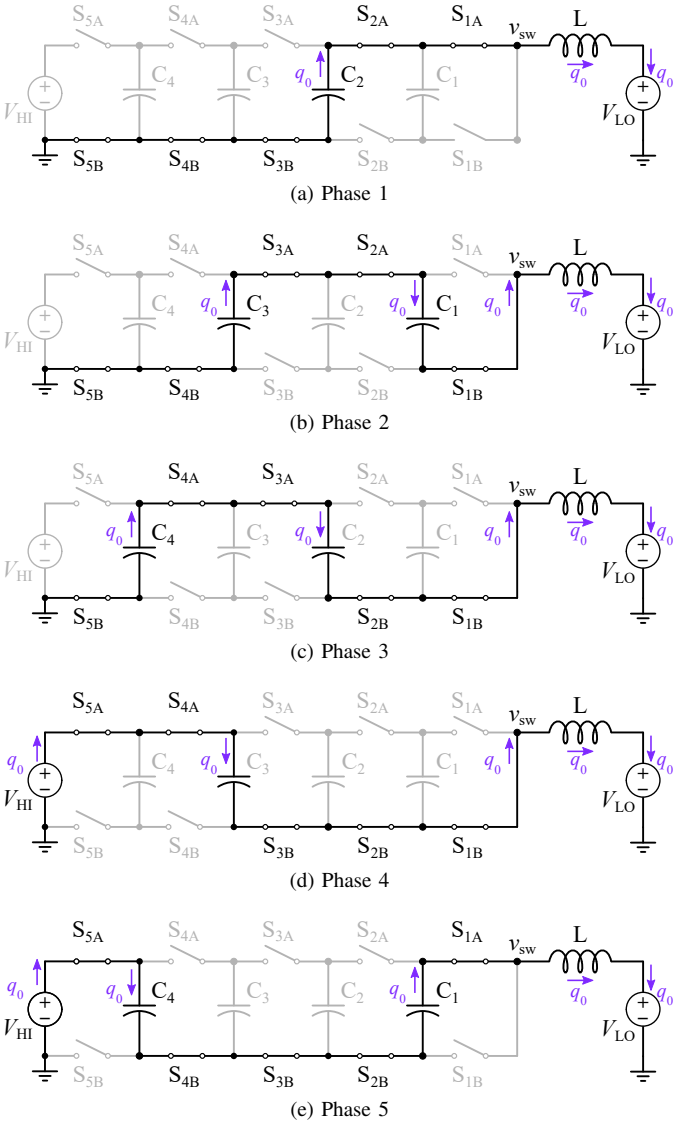

Fig. 4: Schematics illustrating the phase progression of a 5:2 FCML converter, highlighting the charge flow during each phase. All charge flow is expressed in relation to the charge quantity q_0, where $q_{HI} = 2q_0$, and $q_{LO} = 5q_0$.

However, having obtained these phase durations, this work describes the correct phase ordering as a function of M.

A. At Resonance ($\Gamma = 1$)

When operating in a resonant or above-resonant mode for any $N{:}\,M$ conversion ratio, the FCML converter will always have two phases (denoted by '1C') in which the output inductor is connected in series with a single flying capacitor of capacitance C_0. For all other phases (denoted by '2C'), the output inductor is connected in series with two series-connected flying capacitors, with a total effective capacitance $\frac{C_0}{2}$. Using the phase labeling as defined in Fig. 2, Phase 1 and Phase N-M+1 will have only one flying capacitor connected. For the most extreme conversion ratio of $N{:}\,1$, this corresponds to Phase 1 and Phase N. However, for a conversion ratio of 5:2, as shown in Fig. 4, this corresponds

to Phase 1 and Phase 4. In these phases, the undamped natural resonant frequency, $\omega_{0,1C}$, can be calculated from the inductance and effective capacitance using (1). All other phases are topologically equivalent to each other, as they have two series-connected flying capacitors connected with the inductor. The natural resonant frequency in these phases can therefore be calculated using (2) with the relationship between the two resonant frequencies given in (3).

$$\omega_{0,1C} = \frac{1}{\sqrt{LC_0}} \tag{1}$$

$$\omega_{0,2C} = \frac{1}{\sqrt{L \cdot \left(\frac{1}{2}C_0\right)}} \tag{2}$$

$$\sqrt{2}\,\omega_{0,1C} = \omega_{0,2C} \tag{3}$$

While equal charge q_0 flows through the inductor during each phase, the associated capacitor networks have an effective capacitance of either C_0 or $\frac{1}{2}C_0$. As discussed in [16], the time duration of each phase can be given by:

$$\frac{t_{1C}}{T_{sw}} = \frac{\sqrt{2}}{2\sqrt{2}+N-2} \tag{4}$$

$$\frac{t_{2C}}{T_{sw}} = \frac{1}{2\sqrt{2}+N-2} \tag{5}$$

Moreover, the peak current during the single-capacitor phase ('1C') and series-connected-capacitors phase ('2C') must be different. The relationship between the peak inductor currents, $I_{pk_{1C}}$ and $I_{pk_{2C}}$ can be determined using the ratio of their resonant frequencies to be: $\sqrt{2}\,I_{pk_{1C}} = I_{pk_{2C}}$. Exact expressions relating $I_{pk_{1C}}$ and $I_{pk_{2C}}$ to the output current $I_{out} = I_{LO}$ (for the demonstrated step-down converter) were derived in [16]. Figure 3a shows inductor current waveforms for a 5:2 FCML converter operating at resonance, with the peak values labeled.

B. Above Resonance ($\Gamma > 1$)

To concisely describe the FCML converter's operation above resonance, the parameter Γ is defined in (6), and relates the switching frequency f_{sw} (as defined by the full operating period, T_{sw}) to the natural resonant switching frequency $f_{sw,0}$.

$$\Gamma = \frac{f_{sw}}{f_{sw,0}} = \frac{T_{sw,0}}{T_{sw}} \tag{6}$$

The natural resonant switching period, defined by $T_{sw,0} = 1/f_{sw,0}$, is the sum of all phase's resonant half-periods.

When the converter is operated at resonance, Γ is unity, and as the switching frequency increases for above-resonance operation, Γ increases. Example inductor current waveforms for $\Gamma = 2$ and $\Gamma = 100$ are shown in Fig. 3b and Fig. 3c. The $\Gamma = 100$ case is of special interest as it shows that when $f_{sw} \gg f_{sw,0}$, the phase timings converge to equal durations with equal peak currents. To derive the proper duration of each phase for different Γ and $N{:}\,M$ conversion ratios, a 'charge balance' and 'continuous current' constraint between phases are imposed on the inductor current. As shown in [16], an accurate closed-form expression of the relative phase durations t_{1C}/T_{sw} and t_{2C}/T_{sw} can be approximated in (7) and (8) as a function of N and Γ only.

$$\frac{t_{1C}}{T_{sw}} \approx \left(\frac{1}{N} - \frac{\sqrt{2}}{2\sqrt{2}+N-2}\right) \cdot \frac{\Gamma}{\pi}\sin\left(\frac{\pi}{\Gamma}\right) + \frac{\sqrt{2}}{2\sqrt{2}+N-2} \tag{7}$$

$$\frac{t_{2C}}{T_{sw}} \approx \left(\frac{1}{N} - \frac{1}{2\sqrt{2}+N-2}\right) \cdot \frac{\Gamma}{\pi}\sin\left(\frac{\pi}{\Gamma}\right) + \frac{1}{2\sqrt{2}+N-2} \tag{8}$$

For both the at-resonance and above-resonance operation, only the order in which t_{1C} and t_{2C} occur within the switching period is dependent on M. As such, the duration of each phase, t_j, can be defined by (9), independent of Γ. This is further verified in the experimental current waveforms presented in Section IV.

$$t_j = \begin{cases} t_{1C} & \text{for } j = 1 \text{ or } j = N\text{-}M\text{+}1 \\ t_{2C} & \text{otherwise} \end{cases} \tag{9}$$

IV. Experimental Validation

An experimental prototype was built to validate the theoretical timing analysis. The converter was operated in a step-down (buck) mode, in which $V_{HI} = V_{in}$ and $V_{LO} = V_{out}$. Table I lists the components used in the constructed converter, shown in Fig. 5. The gate signals of the switches were controlled with phase durations calculated from (7), (8), and (9). The converter was operated at all possible rational conversions from $N{:}\,1$ to $N{:}\,(N-1)$, using the pattern shown in Fig. 2. First, the converter was tested with a variable input voltage V_{in} and fixed output voltage V_{out}, and then with a fixed V_{in} and variable V_{out}. Operating conditions are summarized in Table II, where $f_{sw,0}$ refers to the natural resonant frequency of the converter at $\Gamma = 1$, and f_{sw} refers to the above-resonant switching frequency for $\Gamma = 1.25$ to 5. The conversion ratios $N{:}\,M = \{5{:}1,\ 5{:}2,\ 5{:}3,\ 5{:}4\}$ correspond to $V_{in} = \{200\,\text{V},\ 100\,\text{V},\ 66.7\,\text{V},\ 50\,\text{V}\}$ for Case 1 and $V_{out} = \{20\,\text{V},\ 40\,\text{V},\ 60\,\text{V},\ 80\,\text{V}\}$ for Case 2. The converter was operated up to a maximum output current of 3 A, so as to operate well under the 7.5 A saturation current limit of the inductor.

Fig. 6 shows the measured and ideal inductor currents for Case 1 for conversion ratios from 5:2 up to 5:4, with the output voltage held constant at 40 V. The converter was tested at switching frequencies corresponding to $\Gamma = \{1,\ 1.33,\ 2\}$. The measured timings and amplitudes match well with the predicted theoretical values, validating the presented analysis. For $\Gamma > 1$ a slight deviation in measured waveforms occurs as a result of realistic non-zero dead-time durations between phase intervals.

Fig. 7 and Fig. 8 show the measured converter efficiency as a function of conversion ratio and Γ, for fixed output voltage and fixed input voltage, respectively. In general, larger M corresponds to higher peak efficiency as a smaller voltage-step-down is performed. In all cases, $\Gamma = 1$ has the highest light-load efficiency, since the converter can operate with ZCS

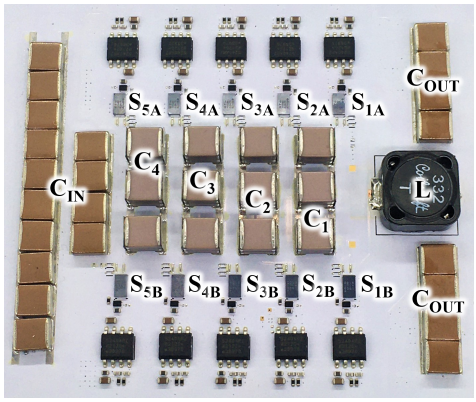

Fig. 5: Photograph of the constructed 5:1 FCML hardware prototype (white soldermask).

TABLE I: Component Details

Component	Description	Part Name
$S_{1\text{-}5A}$, $S_{1\text{-}5B}$	100 V, 3.2 mΩ GaN-FET	EPC2218
$C_{1\text{-}4}$	3 × 0.3 μF, C0G, 250V	CKG57NC0G2E304J500JH
L	3.3 μH	MSS1260-332NLD
R_{GATE}	37.5 Ω, 0402	CR0402-16W-35R7FT
Gate Driver	5 V, 7 A / 5 A	LMG1020
Isolator	Power and Signal	ADUM5240

Given values are nominal; $C_{1\text{-}4}$ and L measured as 935 nF and 3.58 μH for Fig. 6.

and therefore exhibit reduced switching losses. As the load current increases, there is a crossover point at which $\Gamma = 1.25$ becomes the highest efficiency mode. This is near 1 A for Fig. 7 and 1.5 A for Fig. 8. At this load condition, the impact of reducing current ripple and therefore conduction losses is sufficient to outweigh the absence of ZCS above resonance.

In general—for a given load—minimum loss and therefore peak efficiency is achieved when switching losses and conduction losses are balanced. At this first crossover point, Γ values greater than 1.25 yield worse performance, as they exhibit much higher switching losses. At heavier load, however, the efficiency at $\Gamma = 2$ and $\Gamma = 1.25$ are similar. As conduction losses greatly increase, it becomes more advantageous to trade off higher switching losses to reduce rms currents and conduction losses in the converter.

However, there is a point of diminishing returns; operation at $\Gamma = 5$ for all conditions in Fig. 7 and Fig. 8 shows that switching far above resonance results in much worse efficiency performance. This can be understood by comparing the relative trends for switching loss and conduction loss. The rms current depends on both the dc load current as well as the peak-to-peak ripple. Eventually, reducing this ripple has a negligible effect on reducing the overall rms current. This means at these high Γ values (i.e., $\Gamma \geq 5$), the converter is operating with much higher switching losses, without a significant reduction in overall conduction losses. This trend matches the observations in [16] for an $M = 1$ conversion ratio, where the efficiency peaked at different Γ values depending on load current.

In order to verify that the trends in efficiency versus Γ described above are general in nature and not due to the specific distribution of switching loss and conduction loss at each operating condition, testing was done for two separate operating cases. Case 1, shown in Fig. 7, was tested with a fixed output voltage in which output current, and therefore power and conduction losses, remain constant for a given Γ and I_{out} condition. Case 2, shown in Fig. 8, was tested at a fixed input voltage in which switching loss should be consistent across all conversion ratios.

TABLE II: Operating Conditions

Parameter	**Case 1** (Fig. 7)	**Case 2** (Fig. 8)
V_{in}	{200 V, 100 V, 66.7 V, 50 V}	100 V
V_{out}	40 V	{20 V, 40 V, 60 V, 80 V}
$f_{\text{sw},0}$	40 kHz	
$f_{\text{sw}} = \Gamma \cdot f_{\text{sw},0}$	$\Gamma = \{1, 1.25, 1.33^*, 2, 5\}$	

*Only $\Gamma = \{1, 1.33, 2\}$ used for testing in Fig. 6

Fig. 7d shows an operating condition of special interest for 5:4 operation. Here, the maximum output current is limited by the maximum allowable capacitor voltage ripple before the switches undergo reverse conduction. While this limit exists for any given operating condition, it occurs at a lower load current for the $\Gamma = 1$ case because the capacitor voltage ripple is much higher compared to other Γ values, while the dc capacitor voltage remains constant across Γ values.

V. Conclusion

This work has proposed a closed-form solution to determine the timing sequence for operating an N-level FCML converter both at resonance and above resonance, allowing multi-ratio operation for all possible rational conversions $N{:}M$, where $M \in \{1, 2, 3, \ldots, N-1\}$. The experimental prototype shows good agreement with both calculated and simulated phase timing and ordering. Moreover, efficiency measurements provide insight into the benefits of operating above resonance, and show that there is a load-dependent optimal switching frequency that allows for the best trade-off between switching losses and conduction losses.

Acknowledgments

The authors gratefully acknowledge support for this work: Rose Abramson was supported by the U.S. DoD through the National Defense Science & Engineering Graduate (NDSEG) Fellowship Program. Margaret Blackwell was supported by the NSF Graduate Research Fellowship Program under Grant No. DGE-1752814.

References

[1] T. A. Meynard and H. Foch, "Multi-level conversion: high voltage choppers and voltage-source inverters," in *Power Electronics Specialists Conference, 1992. PESC '92 Record., 23rd Annual IEEE*, Jun 1992, pp. 397–403 vol.1.

[2] T. Modeer, N. Pallo, T. Foulkes, C. B. Barth, and R. C. N. Pilawa-Podgurski, "Design of a gan-based interleaved nine-level flying capacitor multilevel inverter for electric aircraft applications," *IEEE Transactions on Power Electronics*, vol. 35, no. 11, pp. 12 153–12 165, 2020.

[3] J. Azurza Anderson, G. Zulauf, P. Papamanolis, S. Hobi, S. Mirić, and J. W. Kolar, "Three Levels Are Not Enough: Scaling Laws for Multilevel Converters in AC/DC Applications," *IEEE Transactions on Power Electronics*, vol. 36, no. 4, pp. 3967–3986, April 2021.

[4] J. T. Stauth, "Pathways to mm-scale dc-dc converters: Trends, opportunities, and limitations," in *2018 IEEE Custom Integrated Circuits Conference (CICC)*, 2018, pp. 1–8.

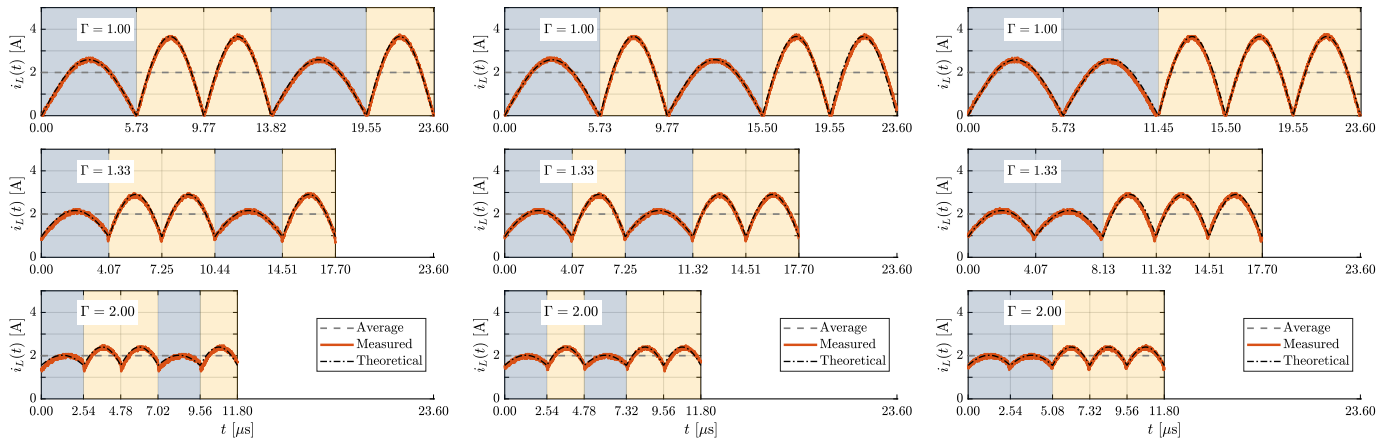

(a) 5:2 (b) 5:3 (c) 5:4

Fig. 6: Measured and calculated inductor current waveforms for a 5-level FCML converter, operating at a) 5:2 b) 5:3 and c) 5:4 conversion ratio. For each mode of operation, the input voltage was varied and the output voltage and power were fixed at 40 V and 80 W, respectively. Phases shaded in blue are single-capacitor phases ('1C'), while phases shaded in yellow are series-connected-capacitors phases ('2C').

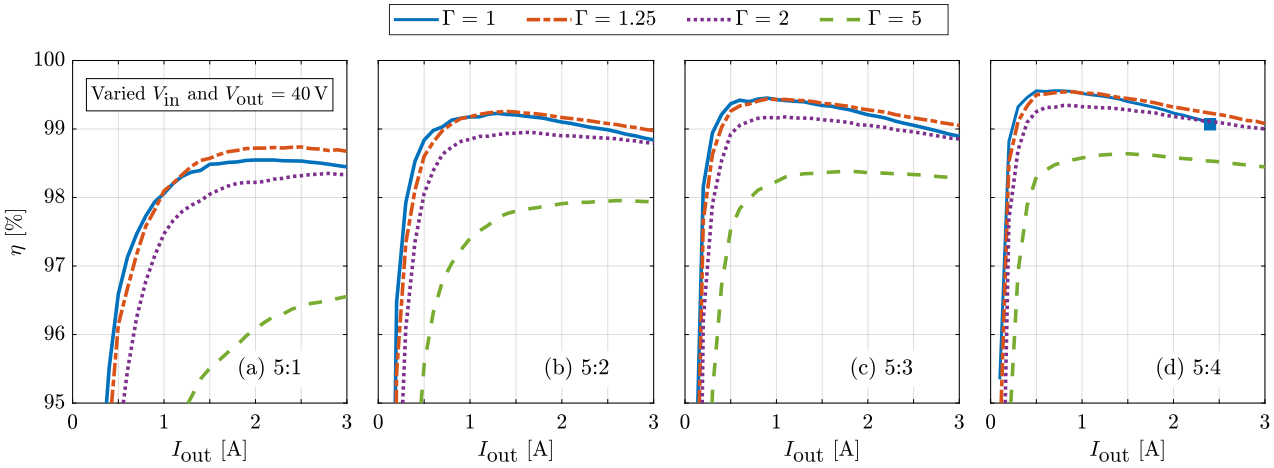

Fig. 7: Measured efficiency for a 5-level FCML converter, operating at a) 5:1 b) 5:2 c) 5:3 and d) 5:4 conversion ratio. For each mode of operation the input voltage, V_{in}, was varied and the output voltage, V_{out}, was kept fixed at 40 V. In d) the square marker denotes the maximum allowable output current, due to excessive capacitor voltage ripple. All efficiency curves were taken in 0.1 A increments.

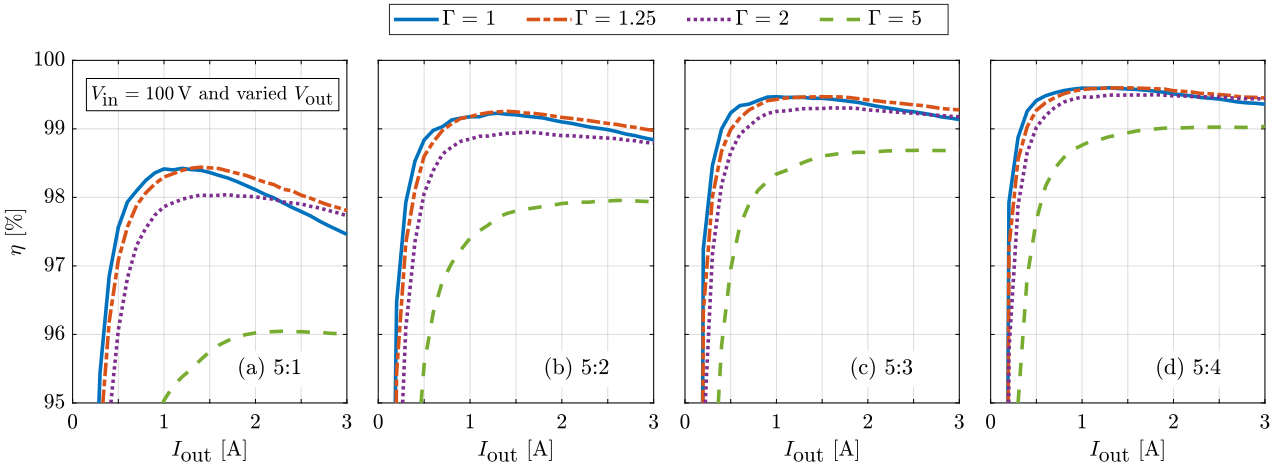

Fig. 8: Measured efficiency for a 5-level FCML converter, operating at a) 5:4 b) 5:3 c) 5:2 and d) 5:1 conversion ratio. For each mode of operation the output voltage, V_{out}, was varied and the input voltage, V_{in}, was kept fixed at 100 V. All efficiency curves were taken in 0.1 A increments.

[5] K. Kesarwani and J. T. Stauth, "Resonant and multi-mode operation of flying capacitor multi-level dc-dc converters," in *2015 IEEE 16th Workshop on Control and Modeling for Power Electronics (COMPEL)*, 2015, pp. 1–8.

[6] C. Schaef, J. Rentmeister, and J. T. Stauth, "Multimode Operation of Resonant and Hybrid Switched-Capacitor Topologies," *IEEE Transactions on Power Electronics*, vol. 33, no. 12, pp. 10 512–10 523, Dec 2018.

[7] W. C. Liu, Z. Ye, and R. C. Pilawa-Podgurski, "Comparative Analysis on Minimum Output Impedance of Fixed-Ratio Hybrid Switched Capacitor Converters," in *2019 20th Workshop on Control and Modeling for Power Electronics (COMPEL)*. IEEE, 2019, pp. 1–7.

[8] Z. Xia, B. L. Dobbins, and J. T. Stauth, "Natural balancing of flying capacitor multilevel converters at nominal conversion ratios," in *2019 20th Workshop on Control and Modeling for Power Electronics (COMPEL)*, 2019, pp. 1–8.

[9] Y. Lei and R. C. N. Pilawa-Podgurski, "A general method for analyzing resonant and soft-charging operation of switched-capacitor converters," *IEEE Transactions on Power Electronics*, vol. 30, no. 10, pp. 5650–5664, 2015.

[10] S. R. Pasternak, M. H. Kiani, J. S. Rentmeister, and J. T. Stauth, "Modeling and Performance Limits of Switched-Capacitor DC–DC Converters Capable of Resonant Operation with a Single Inductor," *IEEE Journal of Emerging and Selected Topics in Power Electronics*, vol. 5, no. 4, pp. 1746–1760, 2017.

[11] Z. Ye, S. Sanders, and R. C. N. Pilawa-Podgurski, "Modeling and Comparison of Passive Component Volume of Hybrid Resonant Switched-Capacitor Converters," *IEEE Transactions on Power Electronics*, 2022.

[12] Z. Ye, Y. Lei, and R. C. Pilawa-Podgurski, "The cascaded resonant converter: A hybrid switched-capacitor topology with high power density and efficiency," *IEEE Transactions on Power Electronics*, vol. 35, no. 5, pp. 4946–4958, 2020.

[13] T. Urkin, G. Sovik, E. E. Masandilov, and M. M. Peretz, "Digital Zero-Current Switching Lock-In Controller IC for Optimized Operation of Resonant SCC," *IEEE Transactions on Power Electronics*, vol. 36, no. 5, pp. 5985–5996, 2020.

[14] M. Seeman and S. Sanders, "Analysis and optimization of switched-capacitor dc-dc converters," *Power Electronics, IEEE Transactions on*, vol. 23, no. 2, pp. 841–851, March 2008.

[15] J. S. Rentmeister and J. T. Stauth, "Modeling the dynamic behavior of hybrid-switched-capacitor converters in state space," in *2018 IEEE 19th Workshop on Control and Modeling for Power Electronics (COMPEL)*, June 2018, pp. 1–7.

[16] N. C. Brooks, S. Coday, M. E. Blackwell, R. A. Abramson, N. M. Ellis, and R. C. N. Pilawa-Podgurski, "Operation of Flying Capacitor Multilevel Converters At and Above Resonance," in *2022 IEEE 23rd Workshop on Control and Modeling for Power Electronics (COMPEL)*, 2022, pp. 1–7.